ACS Sustainable Chemistry & Engineering

Research Article

Cite This: ACS Sustainable Chem. Eng. 2018, 6, 1208−1214

pubs.acs.org/journal/ascecg

Functional Group-Dependent Supercapacitive and Aging Properties of Activated Carbon Electrodes in Organic Electrolyte

Cheng-Hsien Yang,[†] Quoc Dat Nguyen,[†] Ting-Hao Chen,[†] Ahmed S. Helal,[‡,§] Ju Li,[‡] and Jeng-Kuei Chang*[,†,‡]

[†]Institute of Materials Science and Engineering, National Central University, 300 Jhong-Da Road, Taoyuan 32001, Taiwan

[‡]Department of Nuclear Science and Engineering and Department of Materials Science and Engineering, Massachusetts Institute of Technology, 77 Massachusetts Avenue, Cambridge, Massachusetts 02139, United States

[§]Nuclear Materials Authority, P.O. Box 540, El Maadi, Cairo, Egypt

Supporting Information

ABSTRACT: The concentrations of surface functional groups on activated carbon (AC) are manipulated via heat treatment at various temperatures. The carboxyl (O−C = O) population clearly decreases at 600 °C, whereas the lactone (RO−C = O) and phenol (C−OH) populations decrease if the temperature exceeds 750 °C. Their effects on electrode capacitance, leakage current, and gas evolution are systematically investigated in 1 M tetraethylammonium tetrafluoroborate/propylene carbonate electrolyte. The assembled symmetric supercapacitors are also subjected to an aging test, where the cells are held at 2.5 V and 70 °C. The decreased functional group populations significantly reduce gassing and improve the cell durability; the mechanisms are explored using electrochemical impedance spectroscopy and post-mortem SEM. Nevertheless, the AC surface area drops dramatically at 850 °C, resulting in a considerable reduction in capacitance. A rational control of heat-treatment temperature is critical for obtaining AC with balanced supercapacitor performance.

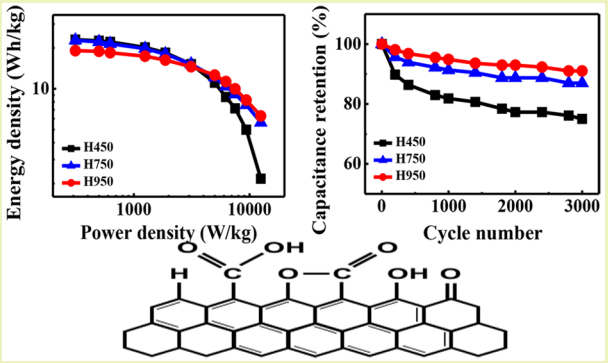

KEYWORDS: *Activated carbon, Supercapacitors, Functional groups, Leakage current, Gas evolution, Aging*

INTRODUCTION

Electric double-layer capacitors (EDLCs) are important charge storage devices owing to their high power density, excellent cycle life, wide operating temperature window, and good charge−discharge efficiency.[1] They have been used in a wide range of applications, such as portable electronic devices, electric vehicles, and grid stabilization.[2] Although a lot of research effort has been devoted to advanced nanostructured materials, such as graphene, carbon nanotubes, and ordered mesoporous carbon,[3,4] activated carbon (AC) is still the most widely used EDLC material in current applications due to its high volumetric capacitance, low cost, and long cycle life.[5] Based on a nonfaradaic charge separation mechanism at the electrode/electrolyte interface, AC electrodes coupled with organic electrolytes (such as propylene carbonate (PC) and acetonitrile based electrolytes) can provide a maximum cell voltage of 2.5−3.0 V, which is higher than most of the pseudocapacitors.[6]

The specific surface area of AC is an important factor for its supercapacitive performance. The surface functional groups on AC are also significant in this regard.[7] Oxygen-containing functional groups such as carboxyl (O−C = O), lactone (RO−C = O), and phenol (C−OH) are usually implanted onto ACs during the activation and subsequent washing processes.[8,9] These groups can enhance electrolyte wettability and aid redox reactions in aqueous electrolytes.[6,10] However, the same chemical activities in organic electrolytes are problematic. Moreover, an excessive amount of oxygen-containing defects can impair the electronic conductivity of AC.[11] It has been reported that the functional groups are unfavorable for cyclic stability of AC electrodes in organic electrolytes.[12,13] The effects of AC surface functional groups on various EDLC properties deserve more systematic investigation, as is carried out in the current work.

Although gravimetric capacitance is usually the focus of most related studies, there are other factors that must be taken into account when practical applications are targeted. For instance, the leakage current of EDLCs that determines the self-discharge rate[12,14] should be considered. Leakage current can lead to energy loss and heat dissipation, complicating thermal management and accelerating EDLC failure. Gassing during operation is another key issue, as this can increase the EDLC internal

Received: September 29, 2017
Revised: November 18, 2017
Published: December 6, 2017

DOI: 10.1021/acssuschemeng.7b03492
ACS Sustainable Chem. Eng. 2018, 6, 1208−1214

pressure, leading to cell rupture and safety threats.[15,16] The evolved gas can also block the pores of the AC and separators, increasing the impedance and resulting in capacitive performance decay.[17] In addition, the aging behavior of AC electrodes is also crucial because long-term stability is expected for any EDLCs.[18] Unfortunately, these properties for ACs with various surface functionalities have rarely been studied in the literature. In the present work, the amount of surface functional groups is carefully manipulated via heat treatment at various temperatures (450−950 °C). The effects on the AC capacitance, leakage current, gas evolution, and aging property (in 1 M tetraethylammonium tetrafluoroborate ($TEABF_4$)/propylene carbonate (PC) electrolyte) are examined for the first time and discussed in detail.

EXPERIMENTAL SECTION

Preparation and Characterization of AC Powder. Pitch was mixed with KOH (in a weight ratio of 1:4) and then heated at 850 °C for 4 h. After being washed by HCl solution and water until the filtrate became neutral, the AC powder was subjected to a postheat treatment in a temperature range of 450−950 °C under N_2 for 2 h, which removed the surface functional groups to various extents. The obtained samples are denoted as H450, H600, H750, H850, and H950 (the numbers indicate the heat treatment temperatures in degrees Celsius). It was found that increasing the heating period to 3 h did not significantly change the functional group populations. The N_2 adsorption/desorption isotherms of the AC samples were measured at 77 K. The specific surface area and total pore volume were then calculated using the quenched solid density functional theory (QSDFT). X-ray photoelectron spectroscopy (XPS) and Boehm titration[19] methods were used to analyze the surface functional groups of various powders. The ACs were also examined using scanning electron microscopy (SEM) and X-ray diffraction (XRD) to characterize the microstructure and crystallinity, respectively.

Electrochemical Measurements. The electrode slurry was prepared by mixing 80 wt % AC powder, 8 wt % carbon black, and 12 wt % poly(vinylidenedifluoride) in *N*-methyl-2-pyrrolidone (NMP) solution. The slurry was pasted onto etched Al foil and vacuum-dried at 120 °C for 3 h. The obtained electrode was then roll-pressed and punched to match the required dimensions of a CR2032 coin cell (the typical thickness of the AC layer was ∼50 μm). Two symmetrical electrodes divided by a cellulose separator were assembled in the coin cell. The electrolyte was composed of 1 M $TEABF_4$ (99 wt %, Alfa Aesar) salt in PC (99.7 wt %, Sigma−Aldrich) solvent. The coin cell was assembled in an argon-filled glovebox (Innovation Technology Co. Ltd.), where both the moisture content and oxygen content were maintained at below 1 ppm.

Galvanostatic charge−discharge tests were performed using a Solartron 1470E potentiostat in a cell voltage range of 0−2.5 V. The leakage current was measured after the cells were held at 2.5 V for 2 h. The gas evolution of the AC cells was evaluated using a homemade electrochemical cell equipped with a pressure gauge (with an accuracy of 0.5 kPa). The cell was galvanostatically charged and then potentiostatically set at 2.5 V for 6 h, while the pressure increase was monitored. The aging tests were performed by holding the cells at 2.5 V and 70 °C. After various durations, the cell performance was evaluated at 25 °C. Electrochemical impedance spectroscopy (EIS) was used to characterize the electrode capacitive behavior upon aging. The electrode morphology and chemical composition changes were examined using SEM and its auxiliary energy dispersive spectroscopy (EDS), respectively.

RESULTS AND DISCUSSION

The metal impurities in the ACs (mainly from the carbon precursor and the chemical activation process) were evaluated by heating the samples in air to 850 °C using a thermogravimetric analyzer. Since the carbon burned out, the amount of residual ash was indicative of the metal impurity level. All the obtained ACs showed ash contents of less than 0.04 wt %, reflecting high purity. Figure 1(a) is the SEM

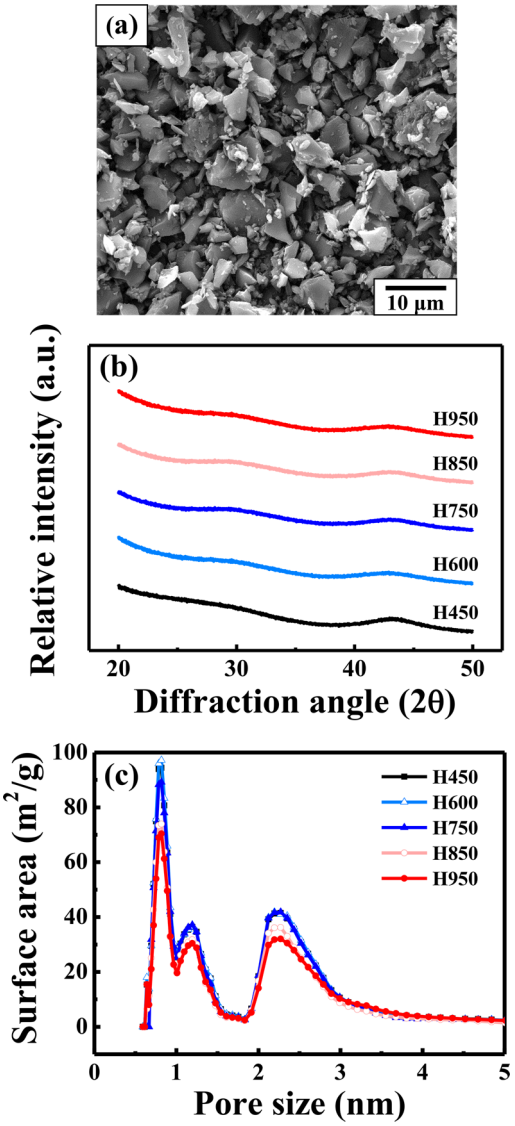

Figure 1. (a) SEM image of H750 powder. (b) XRD patterns and (c) pore size distribution data of various AC samples.

micrograph of H750 powder, showing the AC size is primarily distributed in the range of 5−8 μm. Figure S1 shows the particle size distribution data examined using a laser scattering analyzer. The D_{50} values are approximately 6.3 μm. The ACs treated at other temperatures do not exhibit considerable morphology and size differences, and thus, their data are not shown. The XRD patterns of the samples are shown in Figure 1(b). The ACs did not reveal any distinct diffraction peaks, indicating a lack of a long-range order of atomic periodicity. Figure 1(c) presents the pore size distribution profiles of various ACs. As shown, micropores (with distribution peaks at ∼0.8 and ∼1.2 nm) and mesopores (ranging from 1.9 to 3 nm) coexist. The surface areas of samples heated at or below 750 °C are approximately 1950 $m^2\ g^{-1}$ (Table 1) according to the QSDFT calculation, which is known to be more suitable than the Brunauer−Emmett−Teller calculation for microporous materials.[20] When the temperature increased beyond 750 °C,

DOI: 10.1021/acssuschemeng.7b03492
ACS Sustainable Chem. Eng. 2018, 6, 1208−1214

Table 1. Surface Area and Total Pore Volume of Various AC Samples

	H450	H600	H750	H850	H950
QSDFT surface area ($m^2\ g^{-1}$)	1942	1960	1950	1642	1594
Total pore volume ($cm^3\ g^{-1}$)	0.904	0.919	0.908	0.766	0.756

the surface area (and also the total pore volume; see Table 1) clearly reduced, being less than 1600 $m^2\ g^{-1}$ at 950 °C. As revealed in Figure 1(c), the 0.8 nm peak clearly weakens with a heating temperature higher than 750 °C. This indicates that the micropore structure can be altered by a temperature-induced rearrangement of carbon atoms, leading to a reduction in surface area.

The concentrations of surface functional groups on ACs, as evaluated using the Boehm titration method, are shown in Table 2. The O−C = O groups clearly decreased at 600 °C,

Table 2. Surface Functional Group Concentrations (mmol g^{-1}) on Various AC Samples Evaluated Using the Boehm Titration Method

	H450	H600	H750	H850	H950
C−OH	1.2	1.2	1.2	0.9	0.8
RO−C=O	0.4	0.4	0.4	0.2	0.2
O−C=O	0.8	0.4	0.4	0.3	0.3
Total	2.4	2.0	2.0	1.4	1.3

whereas the RO−C = O and C−OH groups could only be removed if the temperature exceeded 750 °C. The total functional group concentration was reduced from 2.4 mmol g^{-1} for H450 to 1.3 mmol g^{-1} for H950. Figure S2 shows the XPS C 1*s* spectra of various ACs, which confirm coexistence of the C = O, C−OH, COOH, and COOR bonds. Consistent with the Boehm titration results, the XPS data indicate that the oxygen-containing functional groups were eliminated to a greater extent as the heating temperature increased. However, the differences between the XPS spectra were relatively minor. The Boehm titration method seems to be more effective for surface chemistry evaluation of ACs.

Symmetric two-electrode cells were assembled, and their electrochemical properties were evaluated by galvanostatic charging and discharging within a cell voltage V = 2.5 V. Figure 2(a) and (b) shows the voltage profiles of the H750 cell with applied current densities of ±0.5 and ±10 A g^{-1} (based on the AC weight on a single electrode), respectively. Linear and symmetrical charge and discharge branches were observed, indicating ideal capacitive behavior and excellent Coulombic efficiency. The electrode's gravimetric specific capacitance $c_{electrode} \equiv C_{electrode}/m$, where m is the AC mass on one electrode, can be calculated according to[1]

$$C_{electrode} = 2 \times (I \times t)/V \quad (1)$$

where I is the applied current, t is the discharge time, and V is the cell voltage range. The factor of 2 comes from the reasoning that $V = \Delta U^+ - \Delta U^-$, where ΔU^+ and ΔU^- are changes in the absolute potential of the cathode AC and anode AC with respect to some reference electrode. We assume $|\Delta U^+| = |\Delta U^-|$, and $C_{electrode} \equiv Q/|\Delta U^{\pm}|$ is the electrode capacitance where Q is the charge transferred. Table 3 summarizes the $c_{electrode}$ values of various AC electrodes measured at various rates. At a current density of 0.5 A g^{-1}, the capacitances of the H450, H600, H750, H850, and H950 electrodes are 106, 105, 105, 92, and 88 F g^{-1}, respectively. The reduced surface area and pore volume beyond 750 °C (Table 1) are responsible for the decrease in capacitance. An excessive heating temperature is clearly unfavorable with regard to the low-rate capacitance (as well as consuming more manufacturing cost). However, as shown in Table 3, the electrode rate capability improves as the heating

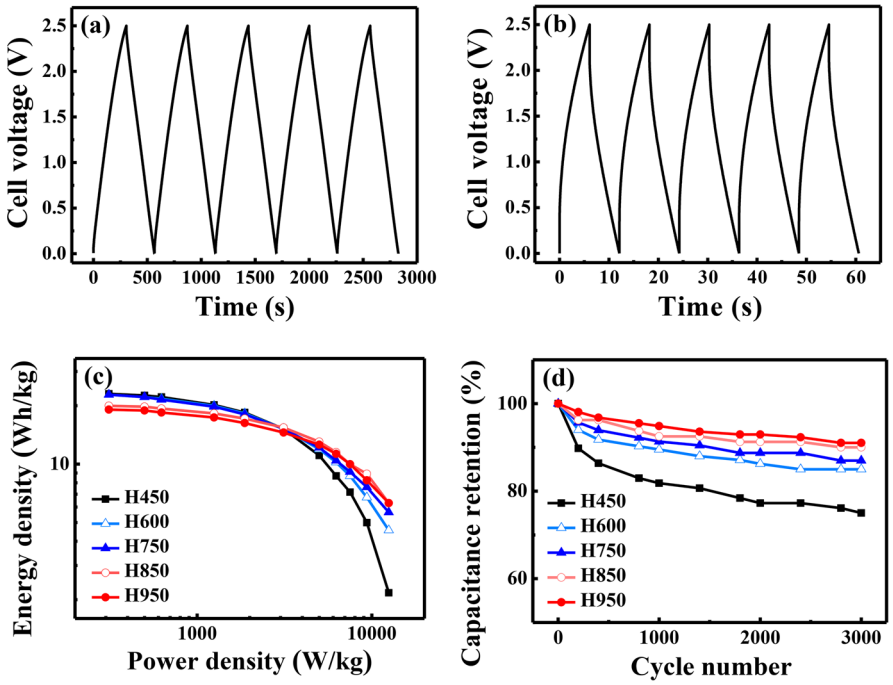

Figure 2. Galvanostatic charge−discharge curves of H750 cell with applied current densities of (a) ± 0.5 and (b) ± 10 A g^{-1}. (c) Ragone plots and (d) cyclic stability data of various AC cells evaluated at 25 °C. The gravimetric normalization is based on the AC weight of both electrodes, 2*m*.

DOI: 10.1021/acssuschemeng.7b03492
ACS Sustainable Chem. Eng. 2018, 6, 1208−1214

Table 3. $C_{electrode}$ Values (F g^{-1}) of Various AC Electrodes Measured at Various Charge−Discharge Rates

Current density (A g^{-1})	H450	H600	H750	H850	H950
0.5	106	105	105	92	88
0.8	104	102	102	91	87
1	101	100	99	89	85
2	93	92	91	84	80
3	85	84	83	79	75
5	70	70	70	71	67
8	51	55	56	60	58
10	40	47	48	53	52
Retention ($c_{10/0.5}$)	38%	45%	46%	58%	59%

temperature increases. The high-rate retention ratios (ratios of the capacitance at 10 A g^{-1} to that at 0.5 A g^{-1}) are 38%, 45%, 46%, 58%, and 59%, respectively. The sheet resistance values, measured using the four-point probe method for the H450, H600, H750, H850, and H950 AC films (without the Al substrates) are 950, 400, 365, 180, and 165 Ω sq^{-1}. A large amount of oxygen content can decrease AC conductivity,[11] which is detrimental to the electrode's rate performance.

The energy density (ED) and power density (PD) of the symmetric full cells can be calculated by the following equations:

$$ED = (c_{cell} \times V^2)/2 \quad (2)$$

$$PD = (c_{cell} \times V^2)/(2 \times t) \quad (3)$$

where $c_{cell} = c_{electrode}/4$ is the cell capacitance based on the total AC weight on both electrodes (the factor of 4 arising from $C_{cell} = C_{electrode}/2$ in eq 1 and the normalizing mass being $2m$). Figure 2(c) shows the Ragone plots of various AC cells. The ED of the H450 cell is 23.0 Wh kg^{-1} at a PD of 0.3 kW kg^{-1}, and it decreases to 2.2 Wh kg^{-1} at 12.5 kW kg^{-1}. For the H950 cell, the ED values are 19.1 Wh kg^{-1} (at 0.3 kW kg^{-1}) and 6.3 Wh kg^{-1} (at 12.5 kW kg^{-1}), respectively. As the heat treatment temperature increased, the high-power performance of the cell improved at the expense of the ED because the AC surface area decreased (especially when T > 750 °C). It is noted that still other factors, such as particle size, pore size distribution, crystallinity, and doping elements, which are beyond the scope of this work, can affect the ED and PD of AC electrodes. These subjects deserve further investigations.

The cycling stability of the cells was evaluated by repeating charge and discharge for 3000 cycles at a current of ±5 A g^{-1}. The obtained data are shown in Figure 2(d). The capacitance retention ratios after cycling for the H450, H600, H750, H850, and H950 cells are 75%, 85%, 87%, 90%, and 91%, respectively. The surface functional groups clearly deteriorated the electrode durability. This could be attributed to their irreversible decomposition upon cycling.[21] The more detailed mechanism is discussed later.

The leakage current (I_L) was measured after the cells were charged and held at 2.5 V for 2 h, when a steady-state current was reached. For an ideal capacitor, no leakage current should be detected. The I_L is attributed to reversible or irreversible side reactions of the electrodes with electrolyte, which cause energy loss during capacitor operation. Figure 3(a) indicates that the H450 cell showed the highest I_L value of 8.8 mA g^{-1} among all the cells examined. The reduction in the surface functional group concentration effectively decreased the I_L to 4.4 mA g^{-1} (for the H950 cell). The functional groups on AC not only

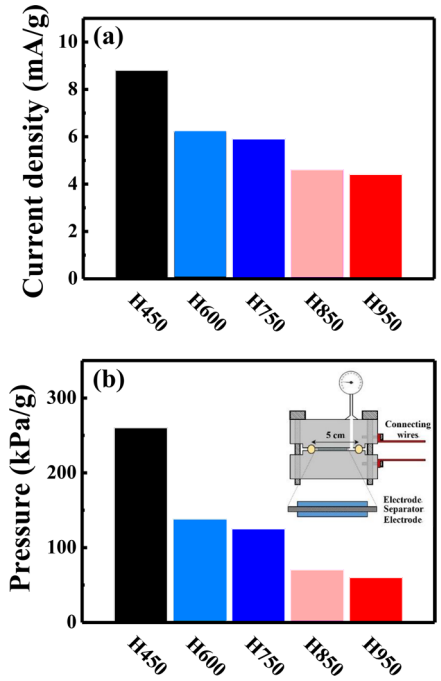

Figure 3. (a) Leakage current density and (b) gas evolution data of various AC cells.

electrochemically break down upon charging[21] but also hinder the formation of a structurally continuous electrode/electrolyte interfacial double layer,[22] leading to the nonideal capacitive behavior. Besides, the oxygen-containing functional groups are highly hydrophilic[23] and thus easily adsorb water, whose electrolysis can also contribute to the I_L.[21]

The homemade cell for gas evolution measurements is illustrated in the inset of Figure 3(b), which shows the data acquired for various cells. The gas generated can deteriorate capacitive performance (like the Leidenfrost effect in boiling) and also lead to mechanical damage including cell rupture and leakage. It can be seen in the figure that the measured pressure decreases significantly from 260 kPa g^{-1} for the H450 cell to 60 kPa g^{-1} for the H950 cell. At the positive electrode, the surface functional groups (i.e., carboxyl, phenol, and ketone) can be oxidized, producing gaseous CO_2 and CO.[21,24] On the anode side, electrolysis of the adsorbed water (by the hydrophilic functional groups) generated H_2 and OH^-, which further reacted with TEA^+ to form ethylene.[25] In addition, PC hydrolysis created CO.[21] As a consequence, decreasing the surface functional group populations suppressed gassing. This trend closely coincides with the leakage current data shown in Figure 3(a).

The aging properties of various ACs were evaluated by holding the cells at 2.5 V and 70 °C, where the electrode deterioration was accelerated. As shown in Table 4, the H450, H750, and H950 cells retain 66%, 80%, and 87% of their initial capacitances, respectively, after 100 h. This trend is quite consistent with the cell cyclability found at 25 °C (Figure 2(d)), suggesting a similar fading mechanism. Figure 4 shows the EIS data of the cells after various periods of aging. All the spectra show a semicircle in the high-frequency region, which is related to contact resistance (R_c) between AC particles and at the AC/current collector interface.[26,27] In the medium-frequency region, the straight 45° inclined Warburg line is attributed to the ion migration impedance through the AC

DOI: 10.1021/acssuschemeng.7b03492
ACS Sustainable Chem. Eng. 2018, 6, 1208−1214

Table 4. Electrochemical Property Variations of Various AC Cells upon Aging at 70 °C

	H450 cell		H750 cell		H950 cell	
Aging time (h)	Capacitance retention (%)	*Rc* (Ω)	Capacitance retention (%)	*Rc* (Ω)	Capacitance retention (%)	*Rc* (Ω)
Fresh	100	37	100	17	100	10
50	81	114	89	48	93	28
100	66	169	80	81	87	52

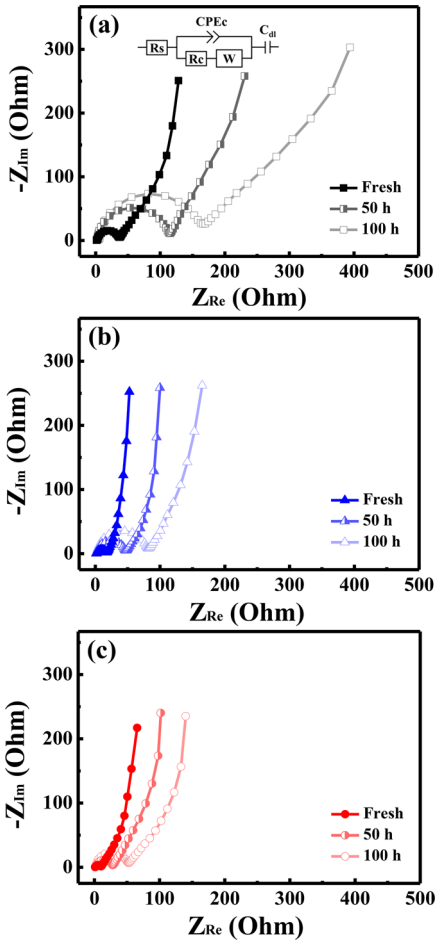

Figure 4. EIS data of (a) H450, (b) H750, and (c) H950 cells before and after various periods of aging at 70 °C.

pores. The nearly vertical line in the low-frequency region represents the capacitive behavior of the EDLC.[28,29] The impedance spectra can be characterized by the equivalent circuit shown in the figure inset, where R_s, CPE_c, W, and C_{dl} are the electrolyte resistance, interfacial constant phase element, Warburg impedance, and double-layer capacitance, respectively. As summarized in Table 4, for the fresh cells, H950 shows the lowest R_c, indicating that the reduced functional group concentration effectively decreases the interface resistance. This also explains the superior high-rate performance of the H950 cell, as described previously. Moreover, Table 4 shows that the R_c values increase with aging time to the largest extent for the H450 cell (from initially 37 to 169 Ω after 100 h). This is attributed to the large gas evolution of this cell (Figure 3(a)), which can lead to separation of AC particles and of the AC/current collector, increasing the electron transport barrier. As also shown in Figure 4, the slope of the low-frequency line significantly decreases upon aging for the H450 cell, suggesting a marked deviation from ideal EDLC behavior. It is found that the property decays (both the semicircle increase and the slope decrease) for the H950 cell are greatly suppressed, indicating a low functional group population is essential to retard the electrode aging rate.

Figure 5 shows the morphologies of the electrodes after 100 h aging. The electrodes were taken out from the cells, cleaned

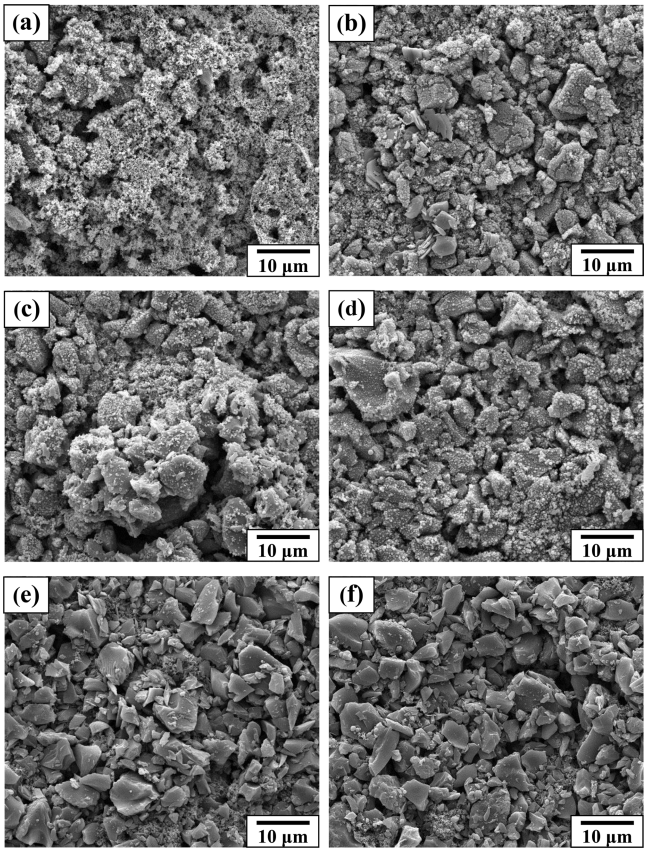

Figure 5. Surface morphologies of (a, b) H450, (c, d) H750, and, (e, f) H950 electrodes after 100 h aging. (a, c, e) Positive electrodes and (b, d, f) negative electrodes.

with PC, and then examined using SEM. The aged electrodes, especially those with lower heating temperatures, are clearly covered by a reaction product layer. This obstacle layer should not only increase the R_c but also hinder the accessibility of AC pores for the electrolyte, resulting in the capacitive performance decay. The EDS data in Table 5 reveal that the aged electrodes are composed of oxygen (O), fluorine (F), and aluminum (Al), besides carbon (C). The C signal is thought to mainly originate from AC. Therefore, according to its intensity, we can know that thicker layers were produced at positive electrodes with lower heating temperatures. The O signal was attributed to oxidation and polymerization of PC,[21] while the F signal originated from the decomposition[29,30] and/or hydrolysis of BF_4^-.[25] The oxygen-containing functional groups and their accompanying adsorbed water could catalyze the above reactions, especially at high potential, leading to the fast degradation of the H450 cell. It is noted that BF_4^- hydrolysis produces F^-, which tends to react with TEA^+ to form HF.[25] This acidic HF can attack the Al current collector, resulting in a corrosion product of AlF_3.[31] This explains the Al signals

DOI: 10.1021/acssuschemeng.7b03492
ACS Sustainable Chem. Eng. 2018, 6, 1208−1214

Table 5. EDS Data (atom %) of Various AC Electrodes before and after Aging at 70 °C for 100 h

	H450 cell			H750 cell			H950 cell		
		Aged			Aged			Aged	
Element	Pristine	Positive	Negative	Pristine	Positive	Negative	Pristine	Positive	Negative
C	93.4	53.1	63.0	94.3	67.4	74.9	95.8	84.1	90.1
O	4.3	18.3	15.0	3.4	13.4	9.0	1.9	4.5	3.2
F	2.3	20.7	16.7	2.3	14.8	12.8	2.3	8.7	5.9
Al	0	7.9	5.3	0	4.4	3.3	0	2.7	0.8

detected on the aged electrodes. Figure 6 compares the underlying Al current collector morphologies of the aged H450 and H950 electrodes (i.e., the AC layers have been removed by NMP). While the H950 Al substrate preserved its original contour (etched Al foil was used), the H450 one was clearly corroded. A large number of deep pits was observed in Figure 6(a), which supports the aforementioned corrosion mechanism. This is the first study that systematically investigates the effects of surface functional groups on the AC aging properties. The results clearly indicate that their concentration should be carefully controlled to ensure the high durability of EDLCs.

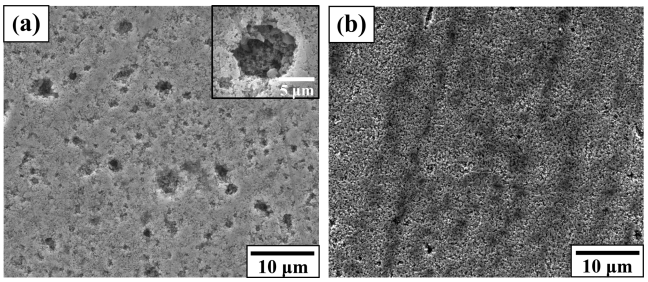

Figure 6. Morphologies of the underlying Al current collectors of (a) H450 and (b) H950 electrodes after 100 h aging at 70 °C.

CONCLUSION

After the activation and subsequent washing processes, the carboxyl (O−C = O), lactone (RO−C = O), and phenol (C−OH) groups were found on the AC surface. These functional groups not only increased R_c, decreasing the electrode rate capability, but also reduced the cyclability. These electrochemically unstable groups and their adsorbed water also led to high leakage current and high gas evolution. The aging tests were performed at a cell voltage of 2.5 V at 70 °C. It was found that the AC with higher functional group populations generated a thicker reaction product layer (composed of O, F, Al, and C), which deteriorated the capacitive performance. The hydrolysis of BF_4^- could subsequently produce HF, which attacked the Al current collector, accelerating the electrode decay. The carboxyl population clearly decreased at 600 °C, whereas the lactone and phenol populations can be reduced at >750 °C. As a consequence, the electrode aging can be effectively suppressed. Nevertheless, a significant drop in the AC surface area was found while heating at 850 °C, which was detrimental for electrode capacitance. Future research intended to further improve practical EDLC performance should look for cost-effective methods to remove oxygen-containing surface functional groups while maintaining the microporous structure of AC.

ASSOCIATED CONTENT

Supporting Information

The Supporting Information is available free of charge on the ACS Publications website at DOI: 10.1021/acssuschemeng.7b03492.

Particle size distribution data of H750 powder, XPS C 1*s* spectra of various AC powders. (PDF)

AUTHOR INFORMATION

Corresponding Author

*Jeng-Kuei Chang. E-mail: jkchang@ncu.edu.tw; jkchang@mit.edu.

ORCID

Ju Li: 0000-0002-7841-8058

Jeng-Kuei Chang: 0000-0002-8359-5817

Notes

The authors declare no competing financial interest.

ACKNOWLEDGMENTS

The financial supports provided for this work by the Ministry of Science and Technology (MOST) of Taiwan and China Steel Corporation of Taiwan are gratefully appreciated. J.L. acknowledges support by NSF ECCS-1610806.

REFERENCES

(1) Conway, B. E. *Electrochemical Supercapacitors: Scientific Fundamentals and Technological Applications*; Springer: New York, 1999. 10.1007/978-1-4757-3058-6.

(2) Beguin, F.; Presser, V.; Balducci, A.; Frackowiak, E. Carbons and electrolytes for advanced supercapacitors. *Adv. Mater.* **2014**, *26*, 2219−2251.

(3) Yan, J.; Wang, Q.; Wei, T.; Fan, Z. J. Recent advances in design and fabrication of electrochemical supercapacitors with high energy densities. *Adv. Energy Mater.* **2014**, *4*, 1300816.

(4) Raccichini, R.; Varzi, A.; Passerini, S.; Scrosati, B. The role of graphene for electrochemical energy storage. *Nat. Mater.* **2014**, *14*, 271−279.

(5) Bose, S.; Kuila, T.; Mishra, A. K.; Rajasekar, R.; Kim, N. H.; Lee, J. H. Carbon-based nanostructured materials and their composites as supercapacitor electrodes. *J. Mater. Chem.* **2012**, *22*, 767−784.

(6) Zhong, C.; Deng, Y. D.; Hu, W. B.; Qiao, J. L.; Zhang, L.; Zhang, J. J. A review of electrolyte materials and compositions for electrochemical supercapacitors,. *Chem. Soc. Rev.* **2015**, *44*, 7484−7539.

(7) Wang, G. P.; Zhang, L.; Zhang, J. J. A review of electrode materials for electrochemical supercapacitors. *Chem. Soc. Rev.* **2012**, *41*, 797−828.

(8) Chen, J. P.; Wu, S. N. Acid/base-treated activated carbons: Characterization of functional groups and metal adsorptive properties. *Langmuir* **2004**, *20*, 2233−2242.

(9) Hall, P. J.; Mirzaeian, M.; Fletcher, I.; Sillars, F. B.; Rennie, A. J. R.; Shitta-Bey, G. O.; Wilson, G. A.; Cruden, R.; Carter, R. Energy

storage in electrochemical capacitors: designing functional materials to improve performance. *Energy Environ. Sci.* **2010**, *3*, 1238−1251.
(10) Kotz, R.; Carlen, M. Principles and applications of electrochemical capacitors. *Electrochim. Acta* **2000**, *45*, 2483−2498.
(11) Polovina, M.; Babic, B.; Kaluderovic, B.; Dekanski, A. Surface characterization of oxidized activated carbon cloth. *Carbon* **1997**, *35*, 1047−1052.
(12) Kierzek, K.; Frackowiak, E.; Lota, G.; Gryglewicz, G.; Machnikowski, J. Electrochemical capacitors based on highly porous carbons prepared by KOH activation. *Electrochim. Acta* **2004**, *49*, 515−523.
(13) Morimoto, T.; Hiratsuka, K.; Sanada, Y.; Kurihara, K. Electric double-layer capacitor using organic electrolyte. *J. Power Sources* **1996**, *60*, 239−247.
(14) Yoshida, A.; Tanahashi, I.; Nishino, A. Effect of concentration of surface acidic functional-groups on electric double-layer properties of activated carbon-fibers. *Carbon* **1990**, *28*, 611−615.
(15) Hahn, M.; Koetz, R.; Gallay, R.; Siggel, A. Pressure evolution in propylene carbonate based electrochemical double layer capacitors. *Electrochim. Acta* **2006**, *52*, 1709−1712.
(16) Zhu, M.; Weber, C. J.; Yang, Y.; Konuma, M.; Starke, U.; Kern, K.; Bittner, A. M. Chemical and electrochemical ageing of carbon materials used in supercapacitor electrodes. *Carbon* **2008**, *46*, 1829−1840.
(17) Jerabek, E. C.; Mansfield, S. F. Method of making an ultracapacitor electrode. U.S. Patent 6,084,766, 2000.
(18) Yu, Z. N.; Tetard, L.; Zhai, L.; Thomas, J. Supercapacitor electrode materials: nanostructures from 0 to 3 dimensions. *Energy Environ. Sci.* **2015**, *8*, 702−730.
(19) Boehm, H. P. Some aspects of the surface-chemistry of carbon-blacks and other carbons. *Carbon* **1994**, *32*, 759−769.
(20) Huang, C. W.; Hsieh, C. T.; Kuo, P. L.; Teng, H. Electric double layer capacitors based on a composite electrode of activated mesophase pitch and carbon nanotubes. *J. Mater. Chem.* **2012**, *22*, 7314−7322.
(21) Ishimoto, S.; Asakawa, Y.; Shinya, M.; Naoi, K. Degradation responses of activated-carbon-based EDLCs for higher voltage operation and their factors. *J. Electrochem. Soc.* **2009**, *156*, A563−A571.
(22) Nian, Y. R.; Teng, H. S. Influence of surface oxides on the impedance behavior of carbonbased electrochemical capacitors. *J. Electroanal. Chem.* **2003**, *540*, 119−127.
(23) Kinoshita, K. *Carbon: Electrochemical and Physicochemical Properties*; John Wiley & Sons, New York, 1988.
(24) Hahn, M.; Wursig, A.; Gallay, R.; Novak, P.; Kotz, R. Gas evolution in activated carbon/propylene carbonate based double-layer capacitors. *Electrochem. Commun.* **2005**, *7*, 925−930.
(25) Kurzweil, P.; Chwistek, M. Electrochemical stability of organic electrolytes in supercapacitors: Spectroscopy and gas analysis of decomposition products. *J. Power Sources* **2008**, *176*, 555−567.
(26) Gualous, H.; Gallay, R.; Alcicek, G.; Tala-Ighil, B.; Oukaour, A.; Boudart, B.; Makany, P. Supercapacitor ageing at constant temperature and constant voltage and thermal shock. *Microelectron. Reliab.* **2010**, *50*, 1783−1788.
(27) Kotz, R.; Ruch, P. W.; Cericola, D. Aging and failure mode of electrochemical double layer capacitors during accelerated constant load tests. *J. Power Sources* **2010**, *195*, 923−928.
(28) Lei, C. H.; Amini, N.; Markoulidis, F.; Wilson, P.; Tennison, S.; Lekakou, C. Activated carbon from phenolic resin with controlled mesoporosity for an electric double-layer capacitor (EDLC). *J. Mater. Chem. A* **2013**, *1*, 6037−6042.
(29) Shen, H. H.; Hu, C. C. Determination of the upper and lower potential limits of the activated carbon/propylene carbonate system for electrical double-layer capacitors. *J. Electroanal. Chem.* **2016**, *779*, 161−168.
(30) Azais, P.; Duclaux, L.; Florian, P.; Massiot, D.; Lillo-Rodenas, M. A.; Linares-Solano, A.; Peres, J. P.; Jehoulet, C.; Beguin, F. Causes of supercapacitors ageing in organic electrolyte. *J. Power Sources* **2007**, *171*, 1046−1053.
(31) Huang, Y. L.; Zhao, Y.; Gong, Q. M.; Weng, M. Y.; Bai, J. F.; Liu, X.; Jiang, Y. Q.; Wang, J. J.; Wang, D. Z.; Shao, Y.; Zhao, M.; Zhuang, D. M.; Liang, J. Experimental and correlative analyses of the ageing mechanism of activated carbon based supercapacitor. *Electrochim. Acta* **2017**, *228*, 214−225.

DOI: 10.1021/acssuschemeng.7b03492
ACS Sustainable Chem. Eng. 2018, 6, 1208−1214